Title: Effective Removal of Silica and Sulfide from Oil Sands Thermal In-Situ Produced Water by Electrocoagulation

Authors: Héline Chow, Anh Le-Tuan Pham

PII: S0304-3894(19)30833-7
DOI: https://doi.org/10.1016/j.jhazmat.2019.120880
Article Number: 120880

Reference: HAZMAT 120880

To appear in: *Journal of Hazardous Materials*

Received date: 14 March 2019
Revised date: 10 June 2019
Accepted date: 8 July 2019

Please cite this article as: Chow H, Pham AL-Tuan, Effective Removal of Silica and Sulfide from Oil Sands Thermal In-Situ Produced Water by Electrocoagulation, *Journal of Hazardous Materials* (2019), https://doi.org/10.1016/j.jhazmat.2019.120880

Effective Removal of Silica and Sulfide from Oil Sands Thermal In-Situ Produced Water by Electrocoagulation

*Héline Chow and Anh Le-Tuan Pham**

Department of Civil and Environmental Engineering

University of Waterloo, Waterloo, Canada

and

Department of Civil and Environmental Engineering

Carleton University, Ottawa, Canada

*Corresponding authors: Anh Le-Tuan Pham (email: anh.pham@uwaterloo.ca; phone: +1-519-888-4567 (ext. 30337)

Graphical abstract

TOC Art

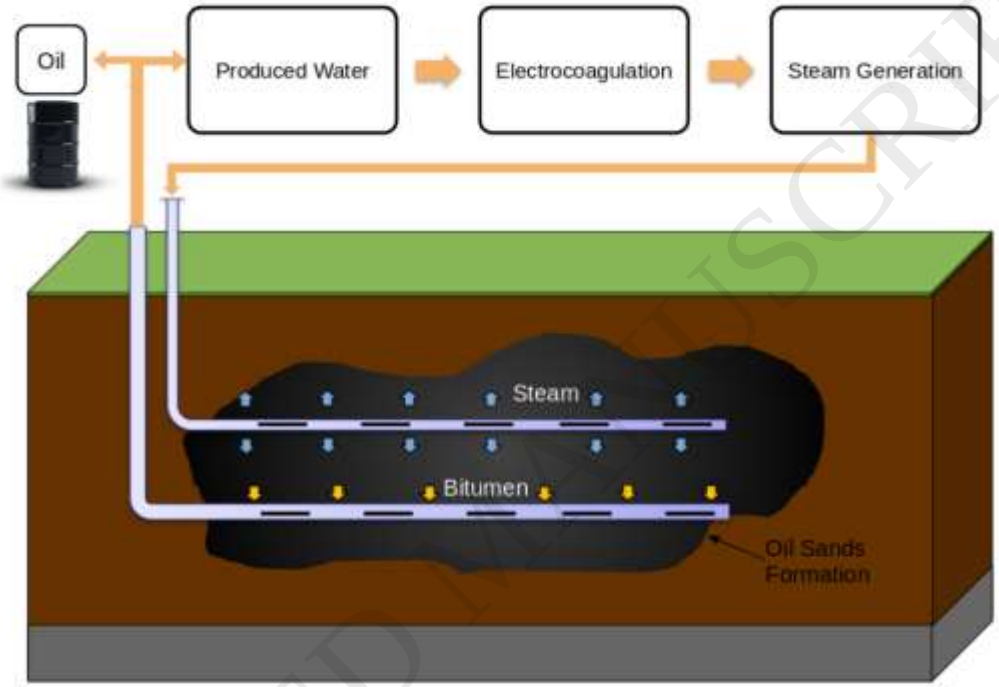

Highlights:

- Electrocoagulation (EC) can remove silica from oil sands in situ produced water
- Fe^0-EC is better than Al^0-EC since the former can also remove sulfide
- In Fe^0-EC, silica removal was attributed to adsorption on FeS precipitates
- Fe^0-EC consumes less energy than evaporative treatment
- Fe^0-EC is a promising technology for the treatment of in situ produced water

Abstract

Effective removal of silica and sulfide from oil sands thermal *in-situ* produced water can reduce corrosion and scaling of steam generators, enhancing water recycling and reuse in the industry. The removal of these two solutes as well as calcium and magnesium (i.e., the solutes that can also cause scaling) from synthetic and authentic produced waters by electrocoagulation (EC) was investigated in this study. In Fe^0-EC, the precipitation of FeS minerals resulted in a rapid removal of sulfide and adsorption of silica onto FeS. In Al^0-EC, silica was removed via adsorption onto aluminum hydroxides, but sulfide was poorly removed. In both EC systems, Ca^{2+} and Mg^{2+} were removed from the organic-free synthetic produced water but not from the authentic water, likely due to the influence of organic species. Contaminant removals in Fe^0-EC were controlled by charge density (q, C/L) but not current density (*i*, mA/cm^2). Overall, this research suggests that EC can be a promising technology for the treatment of thermal *in-situ* produced water. Fe^0-EC appears to be a better choice than Al^0-EC considering that Fe^0-EC was more effective at removing sulfide, and that Fe^0 anodes are usually less expensive.

Key words: Oil sands produced water, electrocoagulation, water treatment

1. Introduction

In-situ thermal recovery technologies such as Steam-Assisted Gravity Drainage (SAGD) and Cyclic Steam Stimulation (CSS) are being increasingly used for the extraction of bitumen in oil sands deposits [1]. These technologies involve the injection of steam into the subsurface to reduce the viscosity of dense bitumen. The oil and steam mixture migrates to the production well and is extracted to the surface. Subsequently, the thermal *in-situ* produced water (i.e., the water produced as a result of steam condensation) is separated from oil, treated and either recycled for steam production or disposed via deep ground injection.

In-situ produced water is comprised of a complex mixture of bitumen residue, dissolved organic compounds, inorganic salts, and suspended solids [2]. Among these constituents, dissolved silica, present at concentrations as high as 350 mg/L, is particularly problematic because its precipitation can lead to scaling of steam generators and clogging of disposal wells. Currently, dissolved silica is removed from the produced water by lime softening or evaporative treatment [2]. However, these treatment technologies have high capital cost, are energy intensive and difficult to operate [3]. Lime softening is also chemical intensive and generates large volume of sludge. Therefore, novel cost-effective technologies that can effectively remove silica are needed to help the oil sands industry increase water recycling, reduce energy consumption and production cost, and reduce environmental impact. To this end, Canada's Oil Sands Innovation Alliance (COSIA) has identified the development of innovative silica removal technologies as one of the industry's priorities [2]. In addition to silica, removing calcium, magnesium, and sulfide from in-situ produced water is also desirable because these solutes can cause scaling and corrosion of pipelines and steam generators [4, 5].

In this study, the treatment of *in-situ* produced water by electrocoagulation (EC) was explored for the first time. EC typically employs electric current to corrode Fe^0 or Al^0 anodes to release Fe(II) (or Al(III)) ions into the solution [6, 7]. These ions then react with solutes in the solution to form Fe-containing (or Al-containing) precipitates that can adsorb a wide variety of contaminants. such as arsenic, chromium, heavy metals, natural organic matter, and viruses [8-13]. Compared with other chemical and biological water treatment technologies, EC offers distinct advantages including no/minimal chemical addition, adjustable/controllable treatment rate, and reduced sludge generation [4. 5].

Several studies have shown that EC can remove silica, sulfide, calcium, and magnesium [14-18], raising the potential of this technology to treat *in-situ* produced water that contains these contaminants. However, these previous studies dealt with wastewater streams (e.g., municipal wastewater, hydraulic fracturing produced water, brackish water, or cooling tower blowdown water) that were less complex than *in-situ* produced water. These studies also often focused on the removal of only one specific contaminant (e.g., sulfide in wastewater, or silica from brackish water) [15, 16]. Whether EC can remove silica, sulfide, calcium or magnesium when these species coexist in a complex water matrix like *in-situ* produced water has not yet been investigated.

We hypothesized that the complex composition of the *in-situ* produced water will greatly influence the performance of EC because the nature of the precipitates generated in EC and the adsorption of contaminants are controlled by the solution chemistry. For example, it has been shown that in oxygenated solutions the precipitates produced by Fe^0-EC were lepidocrocite or a mixture of lepidocrocite and ferrihydrite, whereas magnetite was produced in anoxic solutions [19-20]. In contrast, iron sulfide minerals (FeS) were produced when EC was applied to sulfide-containing waste streams [16, 17]. Because *in-situ* produced water contains up to a few hundred

mg/L of sulfide, it is likely that the precipitates generated by Fe^0-EC treatment would be FeS. However, silica in the *in-situ* produced water may influence the formation of FeS because silica is known to inhibit the precipitation and crystallization of Fe-(hydr)oxides [21, 22]. Therefore, the nature of the precipitates formed during the treatment of in-situ produced water by EC, and whether these precipitates can effectively adsorb contaminants remain to be investigated.

The objective of this study was to determine if EC can be used to remove silica and sulfide, as well as calcium and magnesium, from *in-situ* produced water. Understanding the complex chemical processes that take place in the EC/in-situ produced water system may lead to the development of a more efficient water treatment process for the oil sands industry. To gain insights into the contaminant removal mechanisms, we employed solutions with increasing water chemistry complexity, including 1) synthetic solutions containing only inorganic species (i.e., silica, calcium, magnesium, sulfide, and other inorganic ions); 2) synthetic solutions containing the inorganic species and model organic molecules with functional groups representing those of the organics in the *in-situ* produced water; and 3) authentic *in-situ* produced water which was collected from a heavy oil thermal *in-situ* facility. These solutions were treated by Fe^0-EC and Al^0-EC, employing different current and charge density values. The concentrations of the contaminants, the potentials of the anode and cathode, and the consumption of power were monitored throughout the experiments. Additionally, to identify the nature of the precipitates, a series of characterization techniques such as X-ray Diffraction (XRD), Transmission Electron Microscopy (TEM), Energy Dispersive X-Ray Spectroscopy (EDS), and Selected-Area Electron Diffraction (SAED) were employed.

2. Materials and methods

2.1 Materials

All chemicals were of reagent grade and were used without further purification. All solutions were prepared using 18.2 MΩ·cm water (Millipore System). The electrodes used in the EC experiments were iron rods (d = 4.8 mm, 98%+ purity) and aluminum rods (d = 6 mm, 95.8% purity) obtained from Goodfellow and Metal Supermarkets. Testing solutions included synthetic produced water prepared in the laboratory, and authentic *in-situ* produced water that was collected from a heavy oil thermal *in-situ* facility in Alberta, Canada. The synthetic produced water was prepared daily by dissolving $Na_2SiO_3.9H_2O$, $NaHS.H_2O$, $MgCl_2.6H_2O$, $CaCl_2$, Na_2SO_4, $NaHCO_3$, and NaCl into water to achieve a working solution consisting of approximately 58 mg/L (as Si) dissolved silica, 110 mg/L (as H_2S) sulfide, 65 mg/L Ca^{2+}, 20 mg/L Mg^{2+}, 1700 mg/L HCO_3^-, 1900 mg/L Na^+, 1945 mg/L Cl^-, and 40 mg/L SO_4^{2-}. In some experiments, the solution also contained 5 mM of either 1,3-propanedithiol, cysteine, or glutathione. These model organic compounds were chosen to represent the thiol, carboxylic acid, and amine functional groups of the dissolved organic compounds in the produced water. The pH of the solution was adjusted to 7.6 – 7.8. The composition of the authentic *in-situ* produced water sample is provided in Table S1 of the Supporting Information (SI).

2.2 Electrocoagulation experiment

Experiments were carried out at 22 ± 1ºC in a three-electrode batch cell consisting of 500 mL of reaction solution that was constantly stirred by a magnetic stir bar. The cell was covered with a lid which has three openings that held three electrodes (*i.e.*, working, counter, and reference electrodes), and two more openings for sample subsampling and ORP/pH measurements. The working and counter electrodes (*i.e.*, anode and cathode, respectively) were iron rods (in the Fe^0-

EC experiment) or aluminum rods (in the Al^0-EC experiment), and were placed 1 cm apart. The electrodes were submerged to a depth of 4.8 cm, and therefore the surface area that was exposed to the solution was 6.15 cm^2 ± 0.1 cm (Fe^0 electrodes) and 9.3 cm^2 ± 0.1 cm (Al^0 electrodes). To measure the potential of the anode, a reference electrode (3M NaCl Ag/AgCl, 0.209 V *vs.* SHE) was placed 0.25 cm apart from the anode. The cell was controlled by a VSP potentiostat (Bio-logic Science Instruments). A picture of the experimental setup is provided in the SI (Figure S1).

Before each experiment Fe^0 and Al^0 electrodes were sonicated in water, polished using a sandpaper, and rinsed again with deionized water. Electrocoagulation experiments were conducted under galvanostatic mode (*i.e.*, constant current), employing a current range of 0.05 – 0.8 A. At predetermined time intervals, 10 mL of solution was withdrawn from the reactor and was divided into two aliquots. The first aliquot was filtered through a 0.2-μm syringe filter, and dissolved silica, sulfide, Ca^{2+} and Mg^{2+} were analyzed in the filtrate. The second aliquot was digested with 37 wt. % HCl until all precipitates were dissolved. Subsequently, the digested sample was analyzed for total iron and iron(II). The anode potential and cell voltage, together with the solution pH and ORP, were monitored throughout the course of the experiment. The experiments with synthetic produced water were conducted in triplicate, whereas due to the limited amount of sample available the experiments with authentic produced water were conducted in duplicate. Contaminant concentration profiles were plotted against charge density q (C/L), which represents the electrical charge passed per liter of solution. Charge density is related to current (I) and electrolysis time (t) according to the following equation: $q = \frac{I \times t}{V}$. Therefore, q is proportional to the amount m of iron released into the solution $m = \frac{I \times t \times M}{z \times F} \times \varphi$, where M is the molecular weight of Fe, z is the number of electron involved in the anodic reaction , F is Faraday's constant (96,485 Coulombs/eq), and φ is current efficiency (*i.e.*, the fraction of the charge applied that leads to the

oxidation of Fe). The performance of EC across the 0.05 – 0.8 A current range was evaluated by comparing the contaminant removal at similar *q* values (*i.e.*, at similar amount *m* of iron released). Since longer electrolysis times *t* are required with lower *I* values in order to achieve a similar *q*, the electrolysis time spanned from 19.5 min (for experiments with I = 0.8 A) to 312 min (for experiments with I = 0.05 A). The continuous change in solution volume due to sample sub-sampling (i.e., 10 mL at each time point) was accounted for in all calculations.

2.3 Analytical methods

A Thermo Scientific Orion Ag/AgCl pH electrode and an Ag/AgCl VWR sympHony ORP/Redox probe were used to measure pH and ORP. Total dissolved iron and dissolved iron(II) were measured using the 1,10-phenanthroline method [23]. Dissolved silica was measured using the molybdosilicate method [24]. Because the presence of sulfide affects the analysis, samples were acidified by HCl and sparged with N_2 to remove all sulfide prior to addition of the $(NH_4)_6MO_7O_{24}$ reagent. Sulfide was measured colometrically using the Cline method [25]. Calcium and magnesium were analyzed on a Thermo Dionex Aquion Ion Chromatograph. An Inductively Coupled Plasma Optical Emission Spectrometer (ICP-OES) was employed to analyze for Si, Ca, Mg and Fe in a subset of samples. Prior to the ICP-OES analysis, samples were acidified and stored in a 3 wt. % HNO_3 solution.

Collection of precipitates for XRD characterization involved filtering samples through a 0.22-μm pore size membrane. The materials deposited on the filter were scrapped out, smeared on a zero-background sample holder, and analyzed for crystal structure on a Rigaku Ultima IV X-ray diffractometer with Cu Kα radiation. The morphology, surface composition, and crystal structure of the precipitates were analyzed using a FEI Tecnai G2 F20 TEM coupled with an EDS detector. Liquid samples containing precipitates were deposited on a TEM grid, blotted with a kimwipes

paper, and allowed to dry at room temperature. Sample preparation for XRD and TEM characterizations was conducted under N_2 atmosphere to minimize oxidation.

3. Results and discussion

3.1 Synthetic in-situ produced water (organic free)

Both Fe^0-EC and Al^0-EC were able to remove dissolved silica, sulfide, calcium and magnesium from the synthetic *in-situ* produced water (Figure 1). The contaminant removal efficiency was dependent on the nature of the contaminant, the amount of charge passed through the reaction cell, and the type of anode employed (i.e., Fe^0 vs. Al^0). At the end of the experiment (i.e., q = 2090 C/L), over 95% of silica and over 99% of sulfide were removed by Fe^0-EC, while only silica was effectively removed (~ 99%) by Al^0-EC. The removal efficiencies of Ca^{2+} (80-85%) and Mg^{2+} (20-25%) were comparable in both EC systems. The following discussion will focus on elucidating the electrochemical (i.e., anodic reactions) and chemical (i.e., precipitation and adsorption) processes taking place in the Fe^0-EC system. Subsequently, Al^0-EC will be briefly discussed and compared with Fe^0-EC.

3.1.1 Anodic reactions in Fe^0-EC. When a current of I = 0.2 A (which corresponds to current density of i = 32.5 mA/cm^2) was applied, the ohmic drop-compensated anodic potential varied between -0.45 and - 0.35 V vs. SHE (Figure S2). This potential range indicates that the predominant anodic reaction in the Fe^0-EC system was the oxidation of Fe^0 to Fe(II) (E_h = -0.44 V) [26]. Consistent with this hypothesis, the amount of Fe(II) released from the anode were 90 - 95% of the theoretical amount (which was calculated by assuming that z = 2 in the Faradaic equation (Figure S3)). Approximately 3% of the iron released from the anode was Fe(III). As such, the anodic reactions in our system could also include the oxidation of Fe^0 and Fe(II) to Fe(III). However, the actual amount of Fe(III) formed from the anodic reactions could not be determined as some of the Fe(III) could have been reduced by HS^- to Fe(II) [27]:

$$Fe(III) + 2\ HS^- = FeS + S^0 + 2\ H^+$$

3.1.2 Removal of sulfide and formation of FeS. As was mentioned earlier, Fe^0-EC was effective at removing sulfide (Figure 1A). At q = 750 C/L (with z = 2, this corresponded to an Fe dose of $Fe/S_{initial}$ = 1.17/1 mol/mol), over 99.9% of the initial sulfide was removed from the synthetic solution. Concurrent with sulfide removal was the formation of black-color precipitates whose morphology and SAED pattern suggest that they are poorly crystalline mackinawite (Figures 2A and 2B). Therefore, the removal of sulfide was attributable to the reaction between Fe(II) and HS^-, which produced FeS mineral [27]:

$$Fe(II) + HS^- = FeS_{(s)} + H^+$$

The nearly complete removal of sulfide at $Fe/S_{initial}$ = 1.17/1 is consistent with the stoichiometry of the above reaction.

TEM analyses revealed that FeS was the only type of iron precipitate produced when q ≤ 750 C/L. At q > 750 C/L (*i.e.*, once all sulfide had been removed), we observed the presence of different phases of Fe-(hydr)oxide, one of which was magnetite (Figure 2D and S4). However, most Fe-(hydr)oxide precipitates lacked a well-defined diffraction pattern (Figure 2E and S5). We also would like to note that, unlike the nanocrystalline mackinawite generated in other studies when Fe(II) reacted with HS^- [28-30], the FeS produced in our experiments lacked well-defined XRD (Figure S6) and Debye-ring patterns (Figure 2B). The amorphous/poorly crystalline nature of the precipitates produced in our study was attributable to the presence of a small amount of oxygen in the solution (< 0.5 mg/L) [31], and the presence of silica, a solute known to inhibit the formation, growth, and crystallization of iron minerals [21, 22]. Because more than 97% of the Fe in the precipitates were Fe(II) (Figure S3), the Fe-(hydr)oxides must be Fe^{II}-(hydr)oxides (*e.g.*, green rust type of minerals). Throughout the course of the experiment, the solution remained anoxic (DO

< 0.5 mg/L, ORP < -200 mV, Figure S7), a condition that has been shown to favor the formation of magnetite and green rust [19].

Also present among the precipitates was elemental sulfur (S^0, Figures 2F and S8). S^0 could have been produced from the anodic oxidation of HS^-, and/or from reactions in the bulk solution:

Anodic oxidation: $HS^- = S^0 + 2e^- + H^+$ (E_h = -0.23 V) [32]

Bulk solution reaction: $Fe(III) + 2\ HS^- = FeS + S^0 + 2\ H^+$

3.1.3 Removal of silica, calcium, and magnesium. The concentration of dissolved silica in the synthetic solution gradually decreased as charge was passed through the Fe^0-EC reactor (Figure 1A). Approximately 65% and 95% of the initial silica was removed when q = 750 C/L (*i.e.*, when FeS was the predominant solid phase) and q = 2090 C/L (*i.e.*, when both FeS and Fe-(hydr)oxides were present), respectively. The removal of silica was attributable to the sorption onto FeS at the initial stage, and onto both FeS and Fe-(hydr)oxides at the later stage. Whereas adsorption of silica onto Fe-(hydr)oxides has been well studied [33-37], we are not aware of any reports of adsorption of silica onto FeS. Nevertheless, the removal of silica via other mechanisms cannot be excluded. For example, because the EDS spectrum of the FeS precipitates (Figure 2C) consisted of Si, Fe, and Ca peaks, it could be possible that silica was removed via the precipitation of silicate minerals (*e.g.*, Ca_2SiO_4 or Fe_2SiO_4). The detailed mechanisms through which silica is removed and factors affecting these processes merit further investigation.

Fe^0-EC was also effective at removing Ca^{2+} from the synthetic produced water as the concentration of Ca^{2+} decreased by over 85% when q = 2090 C/L (Figure 1A). In contrast, only less than 25% of the initial Mg^{2+} was removed. The removal of Ca^{2+} and Mg^{2+} was most likely due to the formation of sparingly soluble minerals such as $CaCO_3$, $CaMg(CO_3)_2$, $MgCO_3$, $Mg(OH)_2$, and others (e.g., silicate minerals). During the experiment, the solution pH increased

from 7.7 to 8.9 (Figure S9). At pH 8.9, speciation calculations predicted that over 99% Mg existed as dolomite, and over 98% Ca existed as dolomite and calcite (Figure S10). However, dolomite does not form at ambient temperature [38-40]. When dolomite was excluded from the calculation, the equilibrium model predicted that 85% Mg existed as magnesite, and 99% Ca existed as calcite (Figure S11). As with dolomite, magnesite does not form at ambient temperature [39, 40]. When both dolomite and magnesite was excluded from the calculation, the model predicted that 100% Mg existed as soluble species.

It is important to mention that the pH reported in this study is the pH of the bulk solution. However, lower and higher pH regions could have been developed in the vicinity of the anode and cathode, respectively. The rates of Ca^{2+} and Mg^{2+} precipitation in these regions could be significantly different from those in the bulk solution [41-43]. For example, $Mg(OH)_2$, which precipitates at pH values greater than 10, could have been formed in the alkaline pH regions in the vicinity of the cathode [43]. While the mechanism through which Mg^{2+} was removed was not entirely clear, the relatively poor removal of Mg^{2+} compared with the removal of Ca^{2+} may have been due to the slower rates of formation of Mg minerals than that of Ca minerals.

3.1.4 Effect of current density on contaminant removal and energy consumption. In EC, whereas coagulant dose is determined by q, coagulant dosing rate is controlled by the electrolysis current I; that is, higher currents result in higher fluxes of Fe(II). Previous studies have reported that with the same charge density, better contaminant removal can be achieved at lower I [43, 44]. This is because of the higher current efficiency φ at lower I and/or the increased contact time between coagulant and contaminants due to longer electrolysis time.

The removal of sulfide, dissolved silica, Ca^{2+} and Mg^{2+} at I = 0.05 – 0.8 A (i = 8.13 – 130 mA/cm^2) was investigated and compared. The results showed that while contaminant removals

were dependent on the Fe dose (*i.e.*, better removal of Si, Ca^{2+} and Mg^{2+} at q = 2090 C/L than at q = 750 C/L), they were not appreciably affected by *i* (Figure 3A and 3B). At q = 2090 C/L, despite the significantly different electrolysis times (t = 19.5, 78, 156, and 312 min with *i* = 8.13, 32.5, 65.0, and 130 mA/cm^2, respectively), a similar removal of silica, Ca, and Mg was achieved in all cases. This observation suggests that the adsorption and/or precipitation of the contaminants took place relatively quickly. The slightly better removal of Mg^{2+} at *i* = 8.13 mA/cm^2 could be due to the longer electrolysis time which allowed for the formation of the slower-forming Mg minerals.

The electrolysis current *I* strongly influenced the energy required during the treatment. For the same silica removal percentage, the cumulative energy consumption, $P = \frac{U \times I \times t}{V}$ (kWh/m^3, with *U* being the cell voltage), increased as I increased (Figure 4). The higher energy demand was the result of the higher cell voltage *U* (Figure S11), which was caused by increased overpotential and ohmic drop.

3.1.5 Comparison of Fe^0-EC with Al^0-EC. As noted above, the most prominent difference between Fe^0-EC and Al-EC^0 was that Al^0-EC was much less effective at removing sulfide (Figure 1). In Fe^0-EC, sulfide was removed via reactions with Fe(II) and Fe(III). Because Al(III) ions do not react with sulfide, the removal in Al^0-EC was most likely due to (1) the stripping of H_2S, which was accelerated by the generation of gas bubbles at the electrodes; and (2) the electrochemical oxidation of sulfide on the anode. (As in the Fe^0-EC experiment, we observed the presence of S^0 among the precipitates formed in Al^0-EC (Figure S12)). At similar charge density values, the removals of silica, Ca^{2+} and Mg^{2+} by Fe^0-EC and Al^0-were comparable (Figures 1), with the removal of Mg^{2+} by Al^0-EC (50%) being slightly better than by Fe^0-EC (20%). The removal of these contaminant was attributable to adsorption onto $Al(OH)_3$ and precipitation of carbonate or hydroxide minerals (Figure S13). However, considering that Fe^0-EC was significantly more

effective at removing sulfide, and that Fe^0 anodes are less expensive than Al^0 anodes, Fe^0-EC appears to be a better choice than Al^0-EC.

3.2 Authentic in-situ produced water, and synthetic in situ produced water containing organics

In addition to the inorganic solutes, *in-situ* produced water consists of organic components including oil, grease, and dissolved organic carbon (TOC 200 – 600 mg/L) [2]. The presence of these components could affect the formation of Fe precipitates, and the adsorption/precipitation of contaminants of interest.

The utility of Fe^0-EC was further examined in a series of experiments that employed an authentic *in-situ* produced water sample, and key observations were as follows. Firstly, the Fe^0-EC treatment was able to remove sulfide from the produced water. Although it was not possible to quantify the concentration of sulfide in the solution as the presence of organic reduced sulfurs interfered with the Cline method, the removal of sulfide was evidenced by the formation of FeS (Figure S14). FeS in fact was the predominant precipitate at all q values employed because iron (hydr)oxides were not observed by TEM. Secondly, as in the synthetic produced water experiments, an excellent removal of silica was achieved. Treatment with a charge density of q = 750 C/L reduced silica concentration by over 60% (Figure 5), producing a treated solution containing less than 25 mg/L Si (i.e., the desirable concentration specified by the oil sands industry) [2]. The energy required to achieve this removal level at I = 0.2 A was estimated at approximately 1.1 kWh/m^3 (Figure S15). At this rate, EC's energy demand is over 10 times less that of the evaporative treatment technology, which typically consumes 10 – 15 kWh/m^3 [46]. Since the energy demand by EC will vary depending on the reactor configuration (e.g., electrode shape, the distance between electrodes, flow condition) and operational parameters (e.g., current

density, retention time), further research is needed to optimize the treatment of produced water by EC and reduce energy consumption.

Thirdly, both Ca^{2+} and Mg^{2+} were not appreciably removed (Figure 5). This was attributable to the complexation of Ca^{2+} by dissolved organic compounds, which inhibited the precipitation of Ca minerals. This hypothesis was supported by an experiment with synthetic water samples that also contained 5 mM of either 1,3-propanedithiol, cysteine, or glutathione. The results of this experiment (Figure S16) showed that the presence of each of these organic compounds inhibited/retarded the removal of Ca^{2+}.

In addition to inhibiting Ca^{2+} removal, it was observed that the organic components influenced the precipitate dynamics. In particular, the precipitates settled much more slowly in the produced water experiments than in the organic-free synthetic water experiments. The precipitates produced in the presence of 1,3-propanedithiol, cysteine, or glutathione also settled at slower rates. This is likely due to the sorption of organic compounds onto the precipitates, which slowed the rate at which the precipitates aggregated into larger flocs. Notably, solution foaming was a common phenomenon in the experiments with the authentic produced water. This was attributable to the foaming of oil and grease caused by the evolution of gas bubbles generated at the electrodes. Foaming often led to incomplete mixing of the solution and, in extreme cases, resulted in precipitate flotation (Figure S17). While foaming could present significant operational challenges, flotation could help separate the precipitates from the treated water (a process commonly referred to as electrochemical flotation [47]). Future research investigating the dynamics of the precipitates in the solution may help determine the most appropriate technology for separating the precipitates from the treated water.

4. Conclusions

This research explored the treatment of oil sands *in-situ* produced water by electrocoagulation, focusing particularly on the removal of silica, sulfide, calcium and magnesium. Major findings and their implications are summarized below:

- Both Fe^0-EC and Al^0-EC were effective at removing silica, which was the contaminant of primary concern, from the synthetic and authentic produced water. The added benefit of Fe^0-EC was that it could also effectively remove sulfide. Therefore, Fe^0-EC seems to be a better choice than Al^0-EC, especially considering that Fe^0 anodes are less expensive than Al^0 ones.
- Compared with the two popular silica removal technologies in the oil sands industry, namely warm/hot lime softening and evaporative treatment, Fe^0-EC consumed less energy than evaporative treatment, and is particularly superior to warm/hot lime-softening because of its ability to remove sulfide. Future research investigating how factors such as reactor configuration and operating parameters influence energy demand will help optimize Fe^0-EC and reduce treatment cost.
- While silica is the primary scalant of concern, removal of Ca^{2+} and Mg^{2+} is also desirable. Both Ca^{2+} and Mg^{2+} were poorly removed from the authentic produced water, so additional research is needed to improve their removal.
- Additional research is also needed to evaluate other issues including scaling of the electrodes, methods of separating precipitates from the treated water, and disposing and managing of the FeS sludge generated from the treatment.
- In Fe^0-EC, silica was removed by adsorption onto FeS, a phenomenon reported here for the first time. Future research is needed to investigate the mechanisms of adsorption (e.g., surface complexation or electrostatic interaction) as well as adsorption kinetics and isotherm. This

further understanding is not only relevant to the Fe^0-EC/produced water system, but it may also help elucidate geochemical processes in the environments where dissolved Fe(II), sulfide, and silica coexist (e.g., anoxic sediments, hydrothermal vents).

Acknowledgement. Funding for this research was provided by the Natural Sciences and Engineering Research Council of Canada (NSERC) and Carleton University's Internal Fund.

Supporting Information. Figures S1-S17, Table S1.

References

1. Alberta Energy. Oil sands production profile: 2004-2014, **2016** http://www.energy.alberta.ca/AU/Publications/Documents/InitiativeOSPP.pdf (accessed on March 14, 2019)

2. Canada's Oil Sands Innovation Alliance, Alternative Silica Removal Technologies, **2014.** https://www.cosia.ca/sites/defaulte/files/attachments/COSIAChallenge Water - Alternative Silica Removal Technologies.pdf (accessed on March 14, 2019).

3. F. Ahmadun; A. Pendashteh; L. Abdullah; D. Biak; S. Madaeni; Z. Abidin, Review of technologies for oil and gas produced water treatment. *Journal of Hazardous Materials*, **2009**, 170, 530-551.

4. E. W. Allen, Process water treatment in Canada's oil sands industry: I. Target pollutants and treatment objectives. *Journal of Environmental Engineering and Science*, **2008**, 7, 123-138.

5. J. S. Smith; D.A. Miller, Nature of sulphides and their corrossive effect on ferrous metals: a review. *British Corrosion Journal*, **1975**, 10,13-143.

6. H. Liu; X. Zhao; J. Qu, Electrocoagulation in Water Treatment. In Electrochemistry for the Environment, Springer: New York, **2010**.

7. M. Y. A. Mollah; P. Morkovsky; J. A. G. Gomes; M. Kesmez; J. Parga; D. L. Cocke, Fundamentals, present and future perspectives of electrocoagulation. *Journal of Hazardous Materials*, **2004**, 114, 199-210.

8. W. Wan; T. J. Pepping, T. Banerji; S. Chaudhari; D. E. Giammar, Effects of water chemistry on arsenic removal from drinking water by electrocoagulation. *Water Research*, **2011**, 1, 384-392.

9. D. Lakshmanan; D. E. Clifford; G. Samanta, Comparative study of arsenic removal by iron using electrocoagulation and chemical coagulation. *Water Research*, **2010**, 19, 5641−5652.

10. C. Pan; L. D. Troyer; J. G. Catalano; D. E. Giammar, Dynamics of chromium (VI) removal from drinking water by iron electrocoagulation. *Environmental Science & Technology*. **2016,** 50, 13502-13510.

11. N. Adhoum; Monser L.; Bellakhal N.; Belgaied J., Treatment of electroplating wastewater containing Cu^{2+}, Zn^{2+}, and Cr(VI) by electrocoagulation. *Journal of Hazardous Materials*, **2004**, 112, 207–213.

12. S. Vasudevan; J. Lakshmi; G. Sozhan, Effects of alternating and direct current in electrocoagulation process on the removal of cadmium from water. *Journal of Hazardous Materials*, **2011**, 1, 26-34.

13. S. Chellam; M.A. Aluminum electrocoagulation as pretreatment during microfiltration of surface water containing NOM: A review of fouling, NOM, DBP, and virus control. *Journal of Hazardous Materials*, **2014**, 304, 490-501.

14. Z. Liao; Z. Gu; M. C. Schulz; J. R. Davis; J. C. Baygents; J. Farrell, Treatment of cooling tower blowdown water containing silica, calcium and magnesium by electrocoagulation. *Water Science and Technology*, **2009**, 60, 2345-2352.

15. W. Den; C. Wang, Removal of silica from brackish water by electrocoagulation pretreatment to prevent fouling of reverse osmosis membranes. *Separation and Purification Technology*, **2008**, 59, 318-325.

16. H. Lin; C. Kustermans; E. Vaiopoulou; A. Prevoteau; K. Rabaey; Z. Yuan; I. Pikaar, Electrochemical oxidation of iron and alkalinity generation for efficient sulfide control in sewers. *Water Research*, **2017**, 118, 114-120.

17. M. Murugananthan; G. B., Raju; S. Prabhakar, Removal of sulfide, sulfate and sulfite ions by electro coagulation. *Journal of Hazardous Materials*, **2003**, B109, 37-44.

18. S. Zhao; G. Huang; G. Cheng; Y. Wang; H. Fu, Hardness, COD and turbidity removals from produced water by electrocoagulation pretreatment prior to reverse osmosis membranes. *Desalination*, **2014**, 344, 454-462.

19. K. L. Dubrawski; C. M. van Genuchten; C. Delaire; S. E. Amrose; A. J. Gadgil; M. Mohseni, Production and transformation of mixed-valent nanoparticles generated by Fe(0) electrocoagulation. *Environmental Science & Technology*, **2015**, 49, 2171-2179.

20. K. L. Dubrawski; M. Mohseni, In-situ identification of iron electrocoagulation speciation and application for natural organic matter (NOM) removal. *Water Research*, **2013**, 47, 5371−5380.

21. P. R. Anderson; M. M. Benjamin, Effect of silicon on the crystallization and adsorption properties of ferric oxides. *Environmental Science & Technology*, **1985**, 19, 1048−1053.

22. R. M. Cornell; R. Giovanoli; P. W. Schindler, Effect of silicate species on the transformation of ferrihydrite into goethite and hematite in alkaline media. *Clays and Clay Minerals*, **1987**, 35, 21-28.

23. H. Tamura; K. Goto; T. Yotsuyanagi; M. Nagayama, Spectrophotometric determination of iron(II) with 1,10-phenanthroline in the presence of large amounts of iron(III). *Talanta*, **1974**, 21, 314–318.

24. A.E. Green Berg; L. S. Clesceri; A. D. Eaton, Standard methods for the examination of water and wastewater, **1992**.

25. J.D. Cline, Spectrophotometric determination of hydrogen sulfide in natural waters. *Limnology and Oceanography*, **1969**, 14, 454-458.

26. P. Atkins, Physical Chemistry, 6th edition, W.H Freeman and Company: New York, **1997**.

27. D. Rickard; G. W. Luther III, Chemistry of Iron Sulfides. *Chemical Reviews*, **2007**, 107, 514-562.

28. H. Ohfuji; D. Rickard, High resolution transmission electron microscopic study of synthetic nanocrystalline mackinawite. *Earth and Planetary Science Letters*, **2006**, 241, 227– 233

29. M. Wolthers; S. J. Van Der Gaast; D. Ricard, The structure of disordered mackinawite. *American Mineralogist*, **2003**, 88, 2007–2015.

30. H. Y. Jeong; J. H. Lee; K. F. Hayes, Characterization of synthetic nanocrystalline mackinawite: crystal structure, particle size, and specific surface area. *Geochimica et Cosmochimica Acta*, **2008**, 72, 493-505.

31. D. Csákberényi-Malasics; J. D. Rodriguez-Blanco; V. K. Kis; A. Rečnik; L. G. Benning; M. Pósfai, Structural properties and transformations of precipitated FeS. *Chemical Geology*, **2012**, 294-295, 249–258.

32. M. Bouroushian, Electrochemistry of Metal Chalcogenides. Springer **2010**.

33. G. S. Pokrovski; J. Schott; F. Farges; J.-L. Hazemann, Iron (III)-silica interactions in aqueous solution: insights from X-ray absorption fine structure spectroscopy. *Geochimica et Cosmochimica Acta*, **2003**, 67, 3559−3573.

34. T. Hiemstra; M. O. Barnett; W. H van Riemsdijk, Interaction of silicic acid with goethite. *Journal of Colloid and Interface Science*, **2007**, 310, 8−17.

35. P. J. Swedlund; R. D. Hamid; G. M. Miskelly, Insights into H4SiO4 surface chemistry on ferrihydrite suspensions from ATR-IR, Diffuse Layer Modeling and the adsorption enhancing effects of carbonate. *Journal of Colloid and Interface Science*, **2010**, 352, 149−157.

36. N. Jordan; N. Marmier; C. Lomenech; E. Giffaut; J.-J. Ehrhardt, Sorption of silicates on goethite, hematite, and magnetite: Experiments and modelling. *Journal of Colloid and Interface Science*, **2007**, 312, 224−229.

37. P. J. Swedlund; J. G. Webster, Adsorption and polymerisation of silicic acid on ferrihydrite, and its effect on arsenic adsorption. *Water Research*, **1999**, 33, 3413−3422.

38. J. W. Morse; R. S. Arvidson; A. Luttge, Calcium Carbonate Formation and Dissolution. *Chemical Reviews*. **2007**, 107, 342-381.

39. J. Xu; C. Yan; F. Zhang; H. Konishi; H. Xu; H. H. Teng, Testing the cation-hydration effect on the crystallization of Ca–Mg–CO3 systems. *Proceedings of National Academies of Sciences*, **2013**, 110, 17750-17755.

40. G. Montes-Hernandez; N. Findling; F. Renard; A.-L. Auzende, Precipitation of Ordered Dolomite via Simultaneous Dissolution of Calcite and Magnesite: New Experimental Insights into an Old Precipitation Enigma. *Crystal Growth and Design*, **2014**, 14, 671-677.

41. D. Hasson; G. Sidorenko; R. Semiat, Calcium carbonate hardness removal by a novel electrochemical seeds system. *Desalination*, **2010**, 263, 285-289.

42. S. Zhi; S. Zhang, A novel combined electrochemical system for hardness removal. *Desalination*, **2014**, 349, 68-72.

43. K. Zeppenfeld. Electrochemical removal of calcium and magnesium ions from aqueous solutions. *Desalination*, **2011**, 277, 99-105.

44. K.L. Dubrawski; M. Mohseni, Standardizing electrocoagulation reactor design: Iron electrodes for NOM removal. *Chemosphere*. **2013**, 91, 55-60.

45. P.K. Holt; G.W. Barton; C.A. Mitchell, The future for electrocoagulation as a localised water treatment technology. *Chemosphere*, **2005**, 59, 355–367.

46. Anh Pham's personal communication with Jean Claude Bourgeois (Canadian Natural Resources).

47. X. Chen; G. Chen, Electroflotation. In Electrochemistry for the Environment, Springer: New York, **2010**.

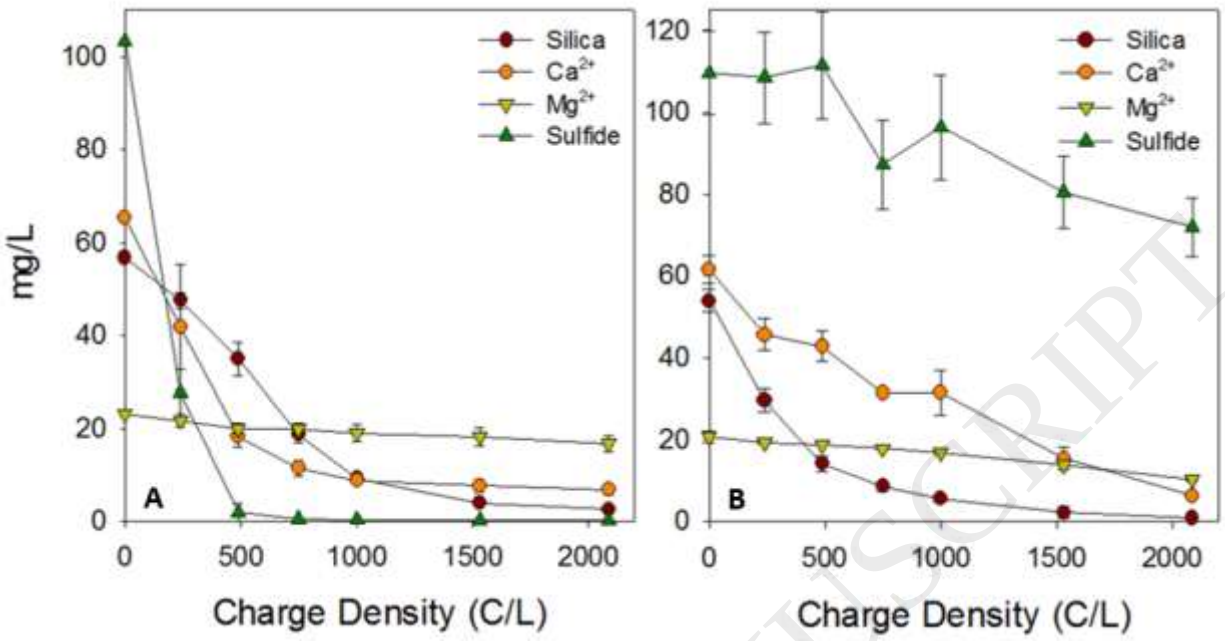

Figure 1. Removal of contaminants from synthetic produced water by Fe^0-EC (A) and Al^0-EC (B). I = 0.2 A (i = 32.5 mA/cm^2).

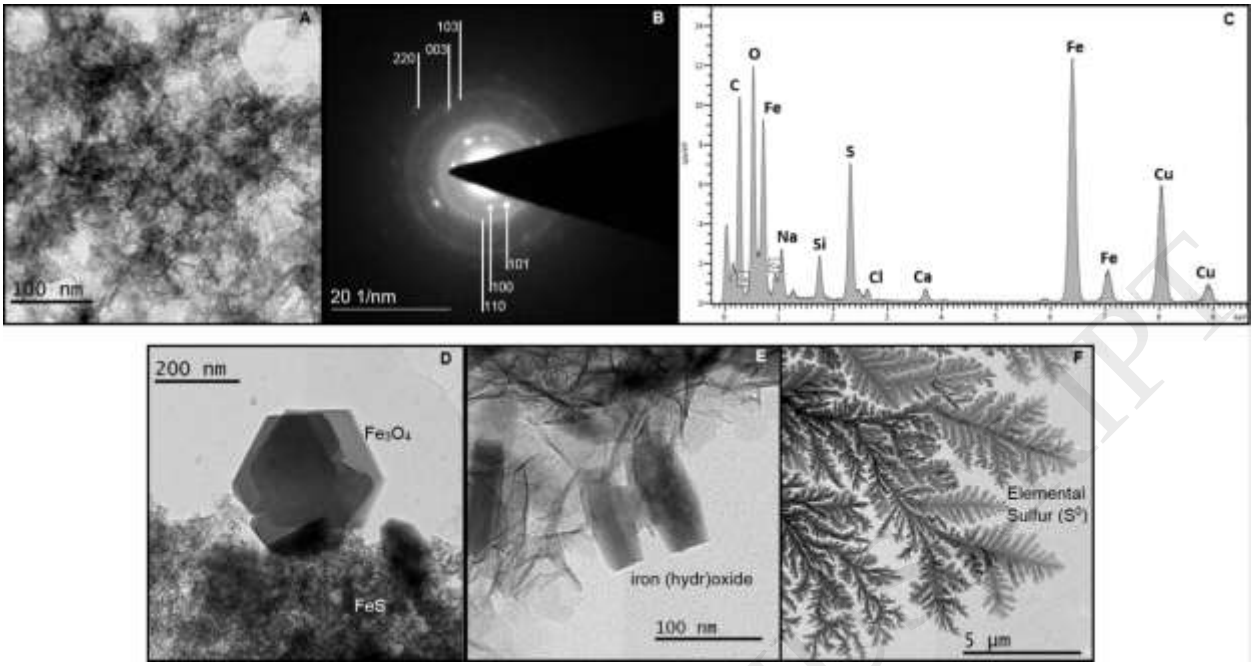

Figure 2. (A-C): TEM image and associated EDS spectrum and SAED pattern of the FeS precipitates formed in the Fe^0-EC experiments with synthetic produced water. Detailed information about the Debye-ring spacings is provided in the SI. **(D-E):** TEM images showing the formation of Fe-(hydr)oxides after all sulfide was removed. The hexagonal-shape precipitate in panel **D** was identified to be magnetite (Fe_3O_4) based on its SAED pattern (Figure S4). The precipitate in panel **E** did not have a well-defined SAED pattern. **(F)** TEM image showing the presence of elemental sulfur (S^0) in the precipitate mixture.

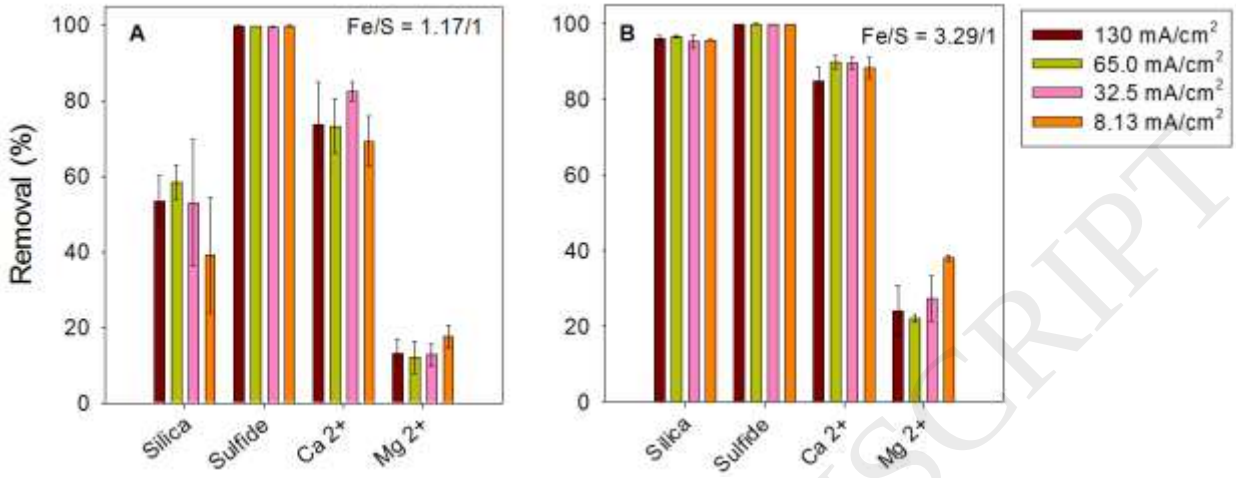

Figure 3. Comparison of contaminant removal at different current densities (i = 8.13 – 130 mA/cm^2) and charge densities (q = 750 C/L and 2090 C/L, which correspond to iron doses of Fe/S_{intial} = 1.17/1 (A) and 3.29/1 (B), respectively).

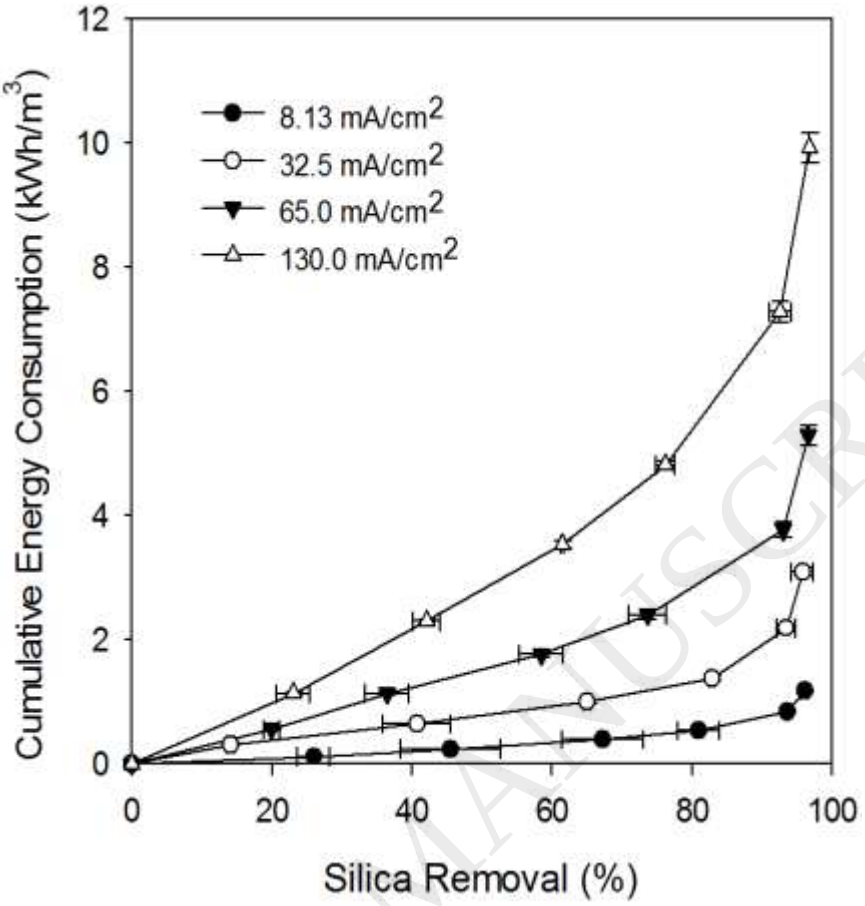

Figure 4. Cumulative energy consumption with increasing silica removal at different current densities.

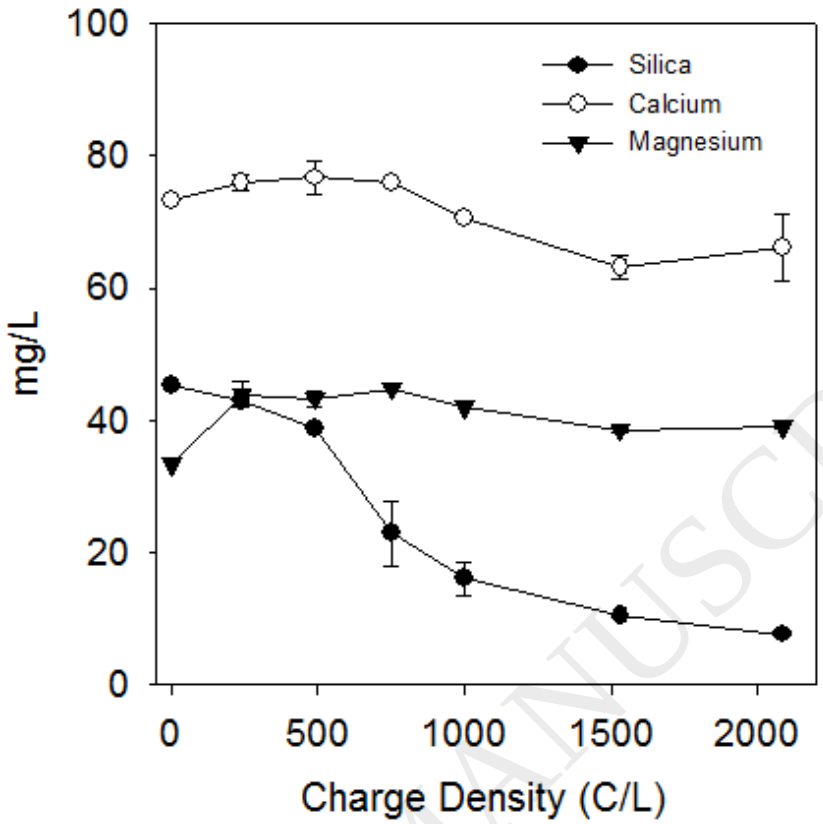

Figure 5. Contaminant **c**oncentration profiles in the Fe^0-EC experiment (I = 0.2 A) with the authentic *in-situ* produced water. Experiments were conducted in duplicate, and the average values along with the range are presented. The increase in the concentrations of Ca^{2+} and Mg^{2+} at the beginning could be due to the presence of high amount of oil and grease in the untreated sample (i.e., corresponding to charge density q = 0 C/L) which interfered with the analysis. The oil and grease components were quickly separated (by foaming) after electric current was passed through the solution, and therefore the subsequent analyses are likely more reliable.